Fine-Resolution Ranging Scheme Based on Signal Strength in Indoor Hallway With Rough-Surface Slab Waveguide

Kyoung-Min Park, Seong-Hwan Hyun, Seongwook Lee, *Member, IEEE*, and Seong-Cheol Kim, *Senior Member, IEEE*

***Abstract*— The received signal strength (RSS) is widely used in range-based localization because of its practical advantages, such as low cost and low complexity. For accurate ranging based on the RSS in indoor environments, well-defined propagation models (PMs) that consider the distortion of the RSS due to abrupt obstructions are required. This article proposes an exponential PM for indoor hallways whose structures can be modeled as a slab waveguide. This waveguide-shaped structure has two main power loss mechanisms: wave penetration and scattering. These loss mechanisms are quantified as exponential coefficients according to the law of conservation of energy. The surface-scattering theory and the multimode waveguide concept are utilized for the quantification of scattering and penetration, respectively. The proposed model is verified through actual site measurements using the vector network analyzer (VNA)-based channel-sounding system at IEEE 802.11ax frequency bands. The estimated range obtained from the measured data indicates that the proposed model leads to the ranging estimation performance that could not be achieved with existing sounding-based indoor channel models.**

***Index Terms*— Channel sounding, indoor channel, indoor localization, range-based localization, received signal strength indicator (RSSI), slab waveguide, wireless measurements.**

I. Introduction

RANGE-BASED localization has been widely studied in recent years because it can be utilized in lots of applications, such as location-based services, target tracking, monitoring, and rescue [1]. In the range-based localization, an accurate ranging estimation should be carried out prior to positioning because the overall performance highly depends on the ranging accuracy. Range pairs between mobile devices can be obtained from time-of-arrival, time-difference-of-arrival, or received signal strength (RSS). The first two methods provide high range estimation accuracy [2], but they have time synchronization issues that require sophisticated hardware [3]. Unlike these methods, RSS-based ranging is more practical due to its simplicity of implementation. Hence, RSS-based ranging is known to be suitable for *ad hoc* wireless networks [4] that are used for state-of-the-art technologies, such as vehicular networks [5], [6] or hyperconnectivity [7].

The accuracy of RSS-based ranging is heavily affected by the propagation environment. Particularly, in indoor environments, various factors causing multipath propagation have to be considered. Thus, propagation models (PMs) considering those factors [8]–[11] are adopted in the RSS-based ranging methods, which are empirically defined for the analysis of communication coverage. The PM is the function of center frequency f_c and propagation distance d. In addition, factors causing signal distortion can be included in the PM. Based on PM, the RSS value can be expressed as

$$P_r = \mathrm{PM}(f_c, d) \tag{1}$$

where P_r is the RSS value that depends on the center frequency and propagation distance. The range can be estimated by obtaining the inverse function of PM. Although existing models are well-defined, they cause significant ranging errors because of their stochastic nature. Often, the fingerprinting method or the ray-tracing simulator [12], [13] can provide relatively accurate RSS values, but they have high computational complexity and exhibit extremely site-specific results.

In most indoor environments, hallway structures commonly appear. Lots of multipaths in the hallway often make the RSS values be unpredictable. Because the indoor hallway environment is a structure with a uniform cross section, a few studies have considered it as a slab waveguide [14], [15]. By solving the wave equation for a slab waveguide, a highly accurate RSS value can be estimated. Unlike fingerprinting or ray-tracing simulators, this approach is generally applicable because most hallways have similar structures. In addition, wave equations can be formulated with simple parameters, such as the width of the hallway and the permittivity of the wall. However, the propagation distance cannot be easily derived from the existing waveguide-based models; therefore, further consideration is required. First, to derive an accurate PM in a practical indoor hallway, several factors for propagation loss must be examined.

1) Medium loss represents the loss of power incurred during propagation. In most indoor environments,

Manuscript received February 18, 2021; revised March 29, 2021; accepted April 5, 2021. Date of publication April 14, 2021; date of current version May 4, 2021. This work was supported in part by a grant to the Bio-Mimetic Robot Research Center funded by the Defense Acquisition Program Administration and in part by the Agency for Defense Development under Grant UD190018ID. The Associate Editor coordinating the review process was Dr. Subhas Chandra Mukhopadhyay. *(Corresponding author: Seong-Cheol Kim.)*

Kyoung-Min Park, Seong-Hwan Hyun, and Seong-Cheol Kim are with the Department of Electrical and Computer Engineering, Seoul National University, Seoul 08826, South Korea, and also with the Institute of New Media and Communications, Seoul National University, Seoul 08826, South Korea (e-mail: rudals319@maxwell.snu.ac.kr; shhyun@maxwell.snu.ac.kr; sckim@maxwell.snu.ac.kr).

Seongwook Lee is with the School of Electronics and Information Engineering, College of Engineering, Korea Aerospace University, Goyang 10540, South Korea (e-mail: swl90@kau.ac.kr).

Digital Object Identifier 10.1109/TIM.2021.3073324

the medium loss is negligible because the wave propagates in an air layer where its conductivity is approximately zero [16].

2) Penetration loss occurs when a wave reflects at a wall and a portion of the wave flows into the wall medium. It can be quantified by calculating the reflection coefficients in a certain guide structure. By addressing multiple deterministic wave paths [17], the total penetration loss can be estimated.
3) Scattering loss occurs when a rough surface induces wave scattering. This phenomenon often causes reflection in unwanted directions. The exponential coefficient for scattering can be modeled by the surface-scattering theory [18], [19].

Based on the assumptions about these losses, we propose a deterministic PM that has a closed-form ranging function for an indoor hallway. A radio wave in a waveguide structure usually undergoes exponential decay [16]. Therefore, the proposed model can be expressed as an exponential function, and its exponential coefficient quantifies the power loss. In addition, the exponential attenuation coefficients for scattering and penetration are calculated. By solving the wave equations which involve the roughness function, transferred power in the rough surface waveguide can be approximated. Besides, deterministic wave paths derive the power loss from the penetration. Based on the law of conservation of energy, the attenuation coefficients are calculated by exploiting the relationship between the guided power and the transferred power. Finally, the proposed exponential PM has a closed-form inverse function for the ranging process. To verify the accuracy of the proposed model, we conduct actual site measurements using the vector network analyzer (VNA). By considering the well-known IEEE 802.11ax standard [20], the measurements are conducted at 2.4- and 5-GHz bands that are widely studied with the measuring manner [21]–[23]. The ranging process with the measured data indicates that the proposed PM is more accurate than existing channel models [8], [9]. Compared to the Indoor Hotspot models of WINNER II, 3GPP, which are widely used for indoor communications, mean ranging errors decrease by about 2 m. This is because the proposed model considers the degree of the roughness according to the frequency bands in indoor environments.

The rest of this article is organized as follows. Section II addresses the overall system model and the propagation mode in an indoor hallway environment. In Section III, the exponential PM for a highly accurate RSS ranging is proposed with an attenuation coefficient estimation. The measurement process and results are presented in Section IV. Finally, we conclude this article in Section V.

II. System Model

A. Hallway Model and Propagation Mode

In a practical *ad hoc* network scenario with low-cost devices, the sidewalls are assumed to have more influence on the wave propagation compared to the ceiling and floor [12]. Therefore, an indoor hallway can be represented as a 2-D slab waveguide. Fig. 1 presents an indoor hallway structure

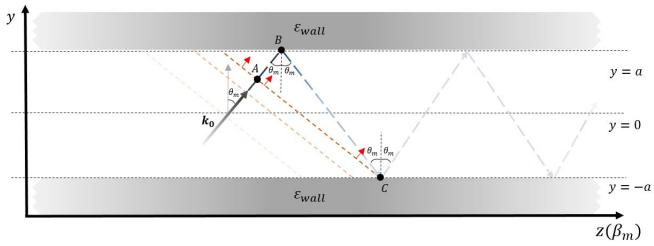

Fig. 1. Slab waveguide modeling for an indoor hallway.

with a width of $2a$. The shaded regions specify the sidewalls, which are assumed to be half-infinite. This presumes that the effective permittivity is equal to the permittivity of the wall, ϵ_{wall}. The unshaded region specifies the air medium with a permittivity of ϵ_0.

In a general guiding structure, there are ray paths in which most of the energy is concentrated. The number of paths equivalent to the mode number is determined by the geometric structure and wavelength. Each mode has specific field properties, such as standing wave pattern, propagation constant, and group velocities. Counting the number of rays that constructively interferes with itself defines the mode number [17]. In Fig. 1, every ray path propagates in the zigzag pattern and has its definitive incident angle with the far-field assumption (i.e., source-free assumption). Among them, some paths build standing wave patterns that are favorable for energy transfer. Assuming a plane wave, following reflections at B and C, the wavefront at C overlaps the wavefront at A. The phase difference between them is $k_0(\overline{\text{AB}}+\overline{\text{BC}})$. When this difference is a multiple of 2π, the energy tends to be concentrated on this path due to the constructive interference. Then, the condition for the incidence angles satisfying it is given as follows:

$$\cos(\theta_m) = \frac{m\lambda}{4a} \quad \left(0 \le \theta_m \le \frac{\pi}{2}\right). \tag{2}$$

This may be thought that two parallel plane waves are in phase. Unless the wavefront of one only after two reflections is in phase with the other, which has not undergone reflection, two interfere destructively with each other. It brings about the same condition with (2). Equation (2) is called the waveguide condition, where $m = 0, 1, \ldots, M$ is an integer and λ is the wavelength of a wave. The hallway described in Fig. 1 has $M+1$ rays capable of propagating without destructive interference. Fig. 2 indicates when there is a certain dominant ray path. The propagation constants along the waveguide direction (i.e., the z-axis direction in Fig. 1) are defined as follows:

$$\beta_m = \frac{2\pi}{\lambda}\sin(\theta_m) \quad (m = 0, 1, \ldots, M). \tag{3}$$

The phasor notation of the electric field for each mode is expressed as follows:

$$E_x(y, z)_m = E_{x0}(y, z)_m \exp(-j\beta_m z) \quad (m = 0, 1, \ldots, M) \tag{4}$$

where $E_{x0}(y, z)_m$ is the standing wave pattern in the smooth-wall waveguide carried by each mode. Equations (3) and (4) imply that each mode carries power independently because each of them has its own group velocity.

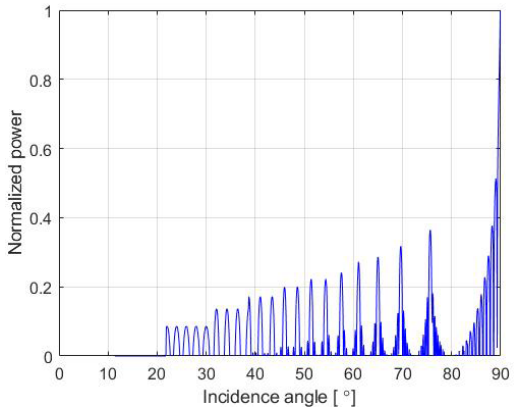

Fig. 2. Delivered power in the smooth-wall indoor hallway (length = 10 m, width = 2 m, and center frequency = 2.4 GHz).

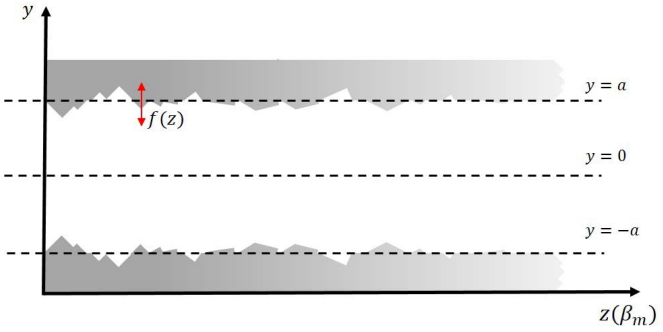

Fig. 3. Indoor hallway with the rough-surface sidewall.

B. Roughness Model

A wave experiences scattered reflection in a rough-surface waveguide, which causes a reflection in an unwanted direction. Power loss inevitably occurs inside the hallway if the sidewalls cause scattering. The degree of roughness depends on the wavelength, which is often judged by some criterion, such as the Rayleigh roughness criterion [24]. The shorter the wavelength, the more it is susceptible to roughness. Roughness is mathematically expressed by the spatial distribution function $f(z)$ [19]. The function $f(z)$ represents the variation from the perfect-smooth wall and is graphically depicted in Fig. 3. For simplicity, it is assumed that the hallway is symmetrical. However, the analysis can be easily extended for unsymmetrical cases [18]. The autocorrelation function [19], which indicates the nature of the roughness, is defined as follows:

$$R(u) \equiv E[f(z)f(z+u)]. \tag{5}$$

The Fourier transform of $R(u)$, denoted as $\widehat{R}(\psi)$, is used to calculate the power loss due to the roughness, as will be discussed in Section III. Generally, the autocorrelation function follows an approximate exponential form for simplicity as follows [19]:

$$R(u) = \sigma^2 \exp\left(-\frac{|u|}{L}\right) \tag{6}$$

where σ^2 is $E[f(z)f(z)]$ that indicates the mean square perturbation, which quantitatively states roughness. In addition, L is the correlation length, which is half of the guide length in general [18].

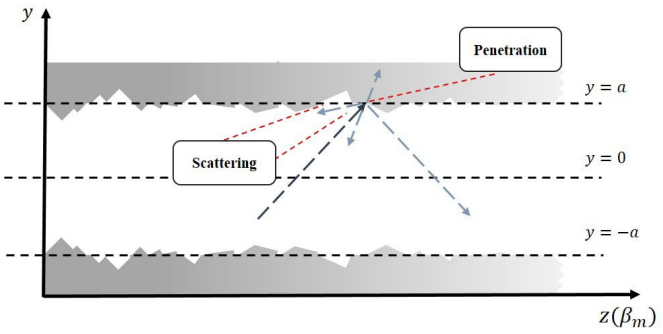

Fig. 4. Two main losses in the guiding structure.

III. PM for Signal Strength-Based Ranging

A. Exponential Propagation Function

In an ideal waveguide, the guided energy is almost completely preserved and transferred. However, several loss mechanisms should be considered in practical situations. Fig. 4 presents two main causes of loss: scattering and penetration. Scattering occurs due to roughness, and penetration stems from the discontinuity of permittivity. Their influences on the power loss are presented as an exponential function as follows:

$$\begin{aligned} P(z) &= P_g \exp(-\alpha_s z)\exp\left(-\alpha_p z\right) \\ &= P_g \exp\left(-\left(\alpha_s + \alpha_p\right)z\right) \\ &= P_g \exp(-\alpha z) \end{aligned} \tag{7}$$

where $P(z)$ is the RSS in the linear scale at distance z, P_g is the guided power, and α_s and α_p indicate the quantification of the scattering and penetration losses, respectively. After receiving the signal with practical devices, range z between the devices could be estimated with the inverse function of (7) as follows:

$$z[m] = \frac{\left(P_g[\text{dB}] - P(z)[\text{dB}]\right)}{4.34\alpha}. \tag{8}$$

The range can also be estimated using the reference distance as follows:

$$z[m] = \frac{(P_0[\text{dB}] - P(z)[\text{dB}])}{4.34\alpha} + 1 \tag{9}$$

where P_0 is the signal strength at the reference distance $z = 1$ m. Ultimately, the coefficient $\alpha = \alpha_s + \alpha_p$ determines the exponent of power loss, and α_s and α_p are discussed in the remainder of this section.

B. Surface Scattering Theory

1) Green's Function: Since $f(z)$ represents the deviation from the smooth-surface wall, the refractive index of the hallway n can be described as follows:

$$n^2 = \epsilon_{\text{wall}} + (1 - \epsilon_{\text{wall}})U[a + f(z) - |y|] \tag{10}$$

where $U[a + f(z) - |y|]$ is the unit step function defined as follows:

$$U[\tau] = \begin{cases} 1, & \tau > 0 \\ 0, & \tau < 0 \end{cases}. \tag{11}$$

Considering these representations, the wave equation for mode m can be written as follows:

$$\nabla^2 E_x(y,z)_m + k_0^2 \epsilon_{\text{wall}} E_x(y,z)_m = k_0^2(\epsilon_{\text{wall}} - 1)U[a + f(z) - |y|]E_{x0}(y,z)_m. \tag{12}$$

The electric field in the right-hand side of (12) could be represented as $E_{x0}(y,z)_m$ because of the unit step function. This approximation deals with a waveguide structure as a volume current source [18]. With the known (i.e., analytically achievable) spatial field, Green's function approach [16] can be used as a general method for solving (12). In radio propagation, Green's function represents the field distribution due to the spatial point source. Therefore, Green's function $G(x, x', y, y')$ for (12) is expressed as follows:

$$\nabla^2 G(y,y',z,z') + k_0^2 \epsilon_{\text{wall}} G(y,y',z,z') = \delta(y-y')\delta(z-z'). \tag{13}$$

The solution for (12) can be written as follows:

$$E_x(y,z)_m = (\epsilon_{\text{wall}} - 1)k_0^2 \int_{-\infty}^{\infty}\int_{-\infty}^{\infty} \big[G(y,y',z,z') \times E_{x0}(y',z')_m U(a + f(z') - |y'|)\big] dy'dz'. \tag{14}$$

It is convenient to analyze (14) in the wavenumber (k_y, k_z) domain. Taking the Fourier transform of (13) renders the Fourier transform of Green's function as follows:

$$\widehat{G}(k_y,k_z) = \frac{\exp(-jk_y y')\exp(-jk_z z')}{\epsilon_{\text{wall}}k_0^2 - k_y^2 - k_z^2}. \tag{15}$$

Because of the unit step function $U[\tau] = 0$ for the wall medium, the even integral (14) can be expressed as follows:

$$E_x(y,z)_m = 2(\epsilon_{\text{wall}} - 1)k_0^2 \times \int_{-\infty}^{\infty} dz' \int_0^{a+f(z')} E_{x0}(y',z')_m G(y,y',z,z')dy'. \tag{16}$$

Since the integration from $y' = 0$ to $y' = a$ makes an imperceptible contribution to the far-field radiation [16], the integration from $y' = a$ to $y' = a + f(z')$ is the only concern. This approximation alludes that only fields near the rough wall have radiation source properties. By a first-order Taylor expansion, for $|f(z')| \ll a$

$$\int_a^{a+f(z')} E_{x0}(y')_m G(y,y',z,z')dy' \simeq E_{x0}(a)_m G(y,a,z,z')f(z') \tag{17}$$

so

$$E_x(y,z)_m \simeq 2E_{x0}(y)_m(\epsilon_{\text{wall}} - 1)k_0^2 \times \int_{-\infty}^{\infty} \exp(-j\beta_m z')G(y,a,z,z')f(z')dz'. \tag{18}$$

The Fourier transform of (18) is expressed as follows:

$$\widehat{E_x}(k_y,k_z)_m = \frac{2E_{x0}(a)_m(\epsilon_{\text{wall}} - 1)k_0^2 \exp(-jk_y a)\widehat{F}(\beta_m + k_z)}{(\epsilon_{\text{wall}}k_0^2 - k_y^2 - k_z^2)} \tag{19}$$

where $\widehat{F}(\beta_m + k_z)$ is the Fourier transform of the wall deviation $f(z)$.

2) Attenuation Coefficient Estimation: To estimate the spatial field domain power, the inverse Fourier transform of (19) should be taken as follows:

$$E_x(y,z)_m \equiv \frac{1}{4\pi^2}\int_{-\infty}^{\infty}\int_{-\infty}^{\infty} \widehat{E_x}(k_y,k_z)_m \times \exp(jk_y y)\exp(jk_z z)dk_y dk_z. \tag{20}$$

From (19), (20) gives

$$E_x(y,z)_m = \frac{2E_{x0}(a)_m}{4\pi^2}k_0^2(\epsilon_{\text{wall}} - 1) \times \int_{-\infty}^{\infty}\int_{-\infty}^{\infty} \frac{e^{-jk_y(y-a)}e^{jk_z z}\widehat{F}(\beta_m + k_z)}{(\epsilon_{\text{wall}}k_0^2 - k_y^2 - k_z^2)}dk_y dk_z. \tag{21}$$

The semicircular contour integral in the complex k_y domain could be used for the integral about k_y in (21), which gives

$$E_x(y,z)_m = -\frac{E_{x0}(a)_m}{2\pi}k_0^2(\epsilon_{wall} - 1) \times \int_{-\infty}^{\infty} \frac{\widehat{F}(\beta_m + k_z)e^{jk_z z - (y-a)p(k_z)}}{p(k_z)}dk_z \tag{22}$$

where $p(k_z)$ is equal to $(\epsilon_{\text{wall}}k_0^2 - k_y^2 - k_z^2)^{0.5}$.

The transformation to the polar coordinate system, which are $z = r\cos(\theta)$ and $y - a = r\sin(\theta)$, and the method of steepest descent [25] make (22) be

$$E_x(r,\theta)_m \simeq \frac{jE_x(a)_m(\epsilon_{\text{wall}} - 1)k_0^2}{(4\pi\sqrt{\epsilon_{\text{wall}}}k_0 r)^{0.5}} \times \widehat{F}(\beta_m - \sqrt{\epsilon_{\text{wall}}}k_0\cos(\theta))\exp^{[j(\pi/4 - \sqrt{\epsilon_{\text{wall}}}k_0 r)]}. \tag{23}$$

Equation (23) indicates the spatial magnitude of each mode. The radiated power carried by each propagation mode is calculated by taking the ensemble average of the magnitude, which is provided as follows:

$$E\big[|E_x(r,\theta)|_m^2\big] = E_x^2(a)_m(\epsilon_{\text{wall}} - 1)^2 \times \int_0^{\pi} \frac{k_0^3}{2\pi\sqrt{\epsilon_{\text{wall}}}} E\Big[|\widehat{F}(\beta_m - \sqrt{\epsilon_{\text{wall}}}k_0\cos(\theta))|^2\Big]d\theta. \tag{24}$$

The ensemble average $E[|\widehat{F}(\psi)|^2]$ is equal to $2L\widehat{R}(\psi)$. This assumption is hold when L is much longer than the wavelength [17], which can be hold in the hallway structure. Using (6), $\widehat{R}(\psi)$ is calculated as follows:

$$\widehat{R}(\psi) = \frac{2\sigma^2 L}{1 + L^2(\psi)^2}. \tag{25}$$

Equation (25) indicates that the radiation is proportional to the mean perturbation. E $[|\widehat{F}(\beta_m - \sqrt{\epsilon_{\text{wall}}}k_0\cos(\theta))|^2]$ in (24)

can be approximated by the Taylor series at $\theta = 0$ for the integration

$$E\left[|\widehat{F}(\beta_m - \sqrt{\epsilon_{\text{wall}}}k_0\cos(\theta))|^2\right] \approx \frac{4\sigma^2 L^2\sqrt{\pi}}{\beta_m L^2 - \sqrt{\epsilon_{\text{wall}}}k_0 L^2 + 1} - \frac{4\sigma^2\theta^2\sqrt{\epsilon_{\text{wall}}}k_0 L^4\sqrt{\pi}}{2\left(\beta_m L^2 - \sqrt{\epsilon_{\text{wall}}}k_0 L^2 + 1\right)^2} + \frac{4\sigma^2\theta^4\sqrt{\epsilon_{\text{wall}}}k_0 L^4\sqrt{\pi}\left(\beta_m L^2 + 5\sqrt{\epsilon_{\text{wall}}}k_0 L^2 + 1\right)}{24\left(\beta_m L^2 - \sqrt{\epsilon_{\text{wall}}}k_0 L^2 + 1\right)^3}. \quad (26)$$

Because each mode has different group velocities, each mode is assumed to carry the power independently. Therefore, the mode number M has not influence on the radiation, and the total radiated power P_r is expressed as follows:

$$P_r = \sum_{m=0}^{M} E\left[|E_x(r,\theta)|_m^2\right]. \quad (27)$$

The attenuation coefficient due to surface scattering α_s is defined by the law of conservation of energy, which is a very usual manner

$$P_r = P_g e^{-\alpha_s 2L} \quad (28)$$

where P_g is the power initially guided as

$$P_g = \frac{\sqrt{\epsilon_{\text{wall}}}}{2}\sqrt{\frac{\epsilon_0}{\mu_0}}\sum_{m=0}^{M}\int_{-\infty}^{\infty} E_x^2(y)_m dy. \quad (29)$$

Finally, α_s is calculated as follows:

$$\alpha_s = \frac{P_r/2L}{P_g}. \quad (30)$$

C. Attenuation Coefficient for Penetration

Reflection and penetration occur under discontinuous permittivity. As shown in Fig. 4, penetration into the wall medium causes a power loss in the waveguide. The amount of energy remaining after reflection depends on the incident angle and permittivity. This is quantified by the reflection coefficient, which is calculated using Snell's law [16] and boundary conditions as follows:

$$\Gamma(\theta_m) = \frac{\cos(\theta_m) - \sqrt{\epsilon_{\text{wall}}}\cos\left(\arcsin\left(\frac{\sin(\theta_m)}{\sqrt{\epsilon_{\text{wall}}}}\right)\right)}{\cos(\theta_m) + \sqrt{\epsilon_{\text{wall}}}\cos\left(\arcsin\left(\frac{\sin(\theta_m)}{\sqrt{\epsilon_{\text{wall}}}}\right)\right)}. \quad (31)$$

Even though the polarization state also influences the reflection coefficient, only transverse-electric (TE) polarization is under consideration because vertical antennas are used for actual site measurements in Section IV. When the normalized power is excited at the boundary, $|\Gamma(\theta_m)|^2$ remains after one reflection. As indicated in Section II, each mode has a definitive incident angle; thus, the power loss can be estimated accurately. If mode m has the initial power P_{m0}, the transferred power P_{mr} after a $2L$ propagation is given as follows:

$$P_{mt} = P_{m0}|\Gamma(\theta_m)|^{2\lfloor L/a\tan(\theta_m)\rfloor} \quad (32)$$

where $\lfloor\cdot\rfloor$ is the floor function that provides the greatest integer, which is less than the input value. Because each mode transfers the power independently, the total transferred power could be simply defined as follows:

$$P_t = \sum_{m=0}^{M} P_{m0}|\Gamma(\theta_m)|^{2\lfloor L/a\tan(\theta_m)\rfloor}. \quad (33)$$

If the initial power P_g in (25) is assumed to be equally distributed for each mode, every P_{m0} has the same value

$$P_{m0} = \frac{\sqrt{\epsilon_{\text{wall}}}}{2(M+1)}\sqrt{\frac{\epsilon_0}{\mu_0}}\sum_{m=0}^{M}\int_{-\infty}^{\infty} E_x^2(y)_m dy. \quad (34)$$

The coefficient α_p can be calculated by the law of conservation of energy, such as α_s

$$\alpha_p = \frac{P_r/2L}{P_g} = 1 - \frac{\sum_{m=0}^{M} P_{m0}|\Gamma(\theta_m)|^{2\lfloor L/a\tan(\theta_m)\rfloor}/2L}{\frac{\sqrt{\epsilon_{wall}}}{2}\sqrt{\frac{\epsilon_0}{\mu_0}}\sum_{m=0}^{M}\int_{-\infty}^{\infty} E_x^2(y)_m dy}. \quad (35)$$

The attenuation coefficient $\alpha = \alpha_s + \alpha_p$ varies according to the geometric and wave properties. The proposed exponential model is verified through actual site measurements in Section IV.

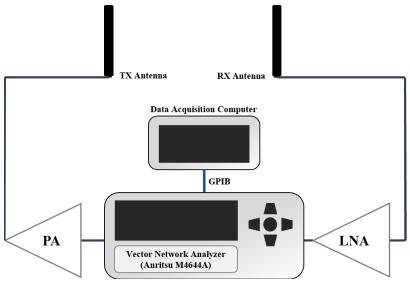

(a)

(b)

Fig. 5. Measurement system. (a) System block diagram. (b) Setup in an indoor hallway.

IV. Validation With Experiments

A. Measurement System

The signal strength was measured in several indoor hallways using the channel-sounding system depicted in Fig. 5. A vector network analyzer (VNA, Anritsu MS4644A) was used for the signal generation and spectrum analysis. This equipment

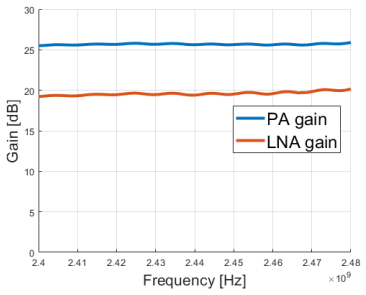

(a)

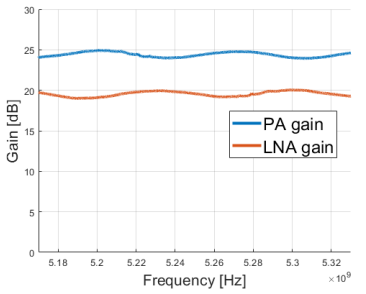

(b)

Fig. 6. Gain measurements of amplifiers with VNA. (a) 2.4–2.48-GHz band. (b) 5.17–5.33-GHz band.

(a) (b) (c)

Fig. 7. Measurement sites. (a) Hallway 1. (b) Hallway 2. (c) Hallway 3.

is able to transmit and receive the wideband signal, which is divided into lots of narrowband tones. Vertical antennas at the transceiver have a 5-dBi gain. The transmitted and received signals are amplified at the power amplifier (PA) and the low-noise amplifier (LNA), respectively. Fig. 6 gives their gains, which are 25 and 20 dB, and shows that the amplifiers have little frequency selectivity. The VNA operates by sweeping the bandwidth and stores the narrowband responses sequentially. The acquired data are conveyed through a general-purpose interface bus (GPIB) cable.

B. Measurement Scenario

1) Measurement Sites: The measurements were conducted at three hallways of the Institute of New Media and Communications (INMC) building of the Seoul National University, as shown in Fig. 7. In indoor building environments, most hallways have structures similar to these experimental environments. Their geometric properties that determine the wave properties are provided in Table I. The hallways have enough lengths to address the statistical term in (24). Despite the presence of windows or doors, which must be considered

TABLE I
GEOMETRIC PROPERTIES OF HALLWAYS

Property	Hallway 1	Hallway 2	Hallway 3
$2a$	2.2 m	2 m	1.8 m
$2L$	9 m	9 m	8 m
σ	0.08 m	0.1 m	0.06 m
ϵ_{wall}	6.283 (2.4 GHz)	6.283 (2.4 GHz)	6.283 (2.4 GHz)
	6.105 (5 GHz)	6.105 (5 GHz)	6.105 (5 GHz)
M	36 (2.4 GHz)	32 (2.4 GHz)	29 (2.4 GHz)
	74 (5 GHz)	67 (5 GHz)	61 (5 GHz)
α_s	0.2306 (2.4 GHz)	0.3622 (2.4 GHz)	0.1303 (2.4 GHz)
	0.4727 (5 GHz)	0.7395 (5 GHz)	0.2655 (5 GHz)
α_p	0.1429 (2.4 GHz)	0.1387 (2.4 GHz)	0.1259 (2.4 GHz)
	0.1439 (5 GHz)	0.1341 (5 GHz)	0.1232 (5 GHz)
α	0.3735 (2.4 GHz)	0.5009 (2.4 GHz)	0.2562 (2.4 GHz)
	0.6166 (5 GHz)	0.8736 (5 GHz)	0.3887 (5 GHz)

in terms of the roughness in each hallway, their dielectric polarizations are neglected because of their relatively small portions. Because the sidewalls in the INMC building are made up of the same concrete-based material that is used in most indoor office buildings, every hallway is assumed to have the same dielectric constant value, which is precisely measured [26]. Two frequency bands that are widely utilized for indoor applications of radio communications are under consideration. The penetration loss has little to do with the frequency band due to the consistency of the dielectric constant. However, the scattering loss is highly influenced by the short wavelength, which causes a frequency dependence of α. In each hallway, data for the ranging process are collected with the measurement system given above.

2) Sounding Specifications: The measurements focus on the IEEE 802.11ax standard [20], which is known as WiFi 6. Hence, the VNA sweeps 2.4–2.48- and 5.17–5.33-GHz bands with 78.125-kHz narrowband tones, which is equal to the subcarrier spacing of WiFi 6. In each hallway, experiments are conducted for each of the two frequency bands. Fig. 8 presents how the transceiver was geometrically addressed. The position of the receiver gradually gets farther from the position of the transmitter radiating 0-dBm power at 1-m intervals. To capture the effect of small-scale fading, each measurement point was divided into eight grids with $\lambda/2$ spacing. The VNA sweeps ten times at one point to obtain ergodicity. At each small grid, all single-tone and short-time data are averaged to suppress the randomness of the measured data, which is conducted based on the maximum likelihood sample estimation with the Gaussian noise assumed. This process is illustrated in Fig. 9. At each measurement point, variations due to small-scale fading are mitigated by averaging all the measured values in small grids.

C. Measurement and Modeling Results

In the performance evaluation, few existing PMs [8], [9] are considered for comparison. They follow the path loss formula, which is widely utilized for RSS ranging because it is easily

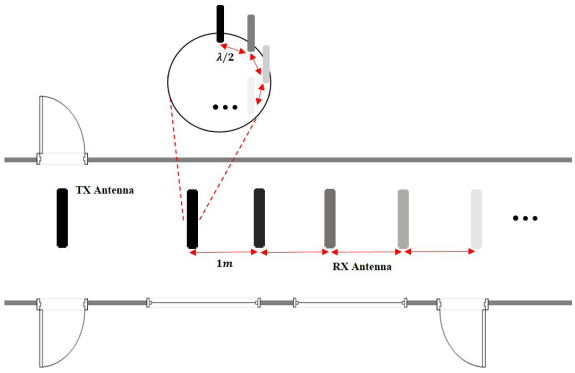

Fig. 8. Geometric location of the transceiver.

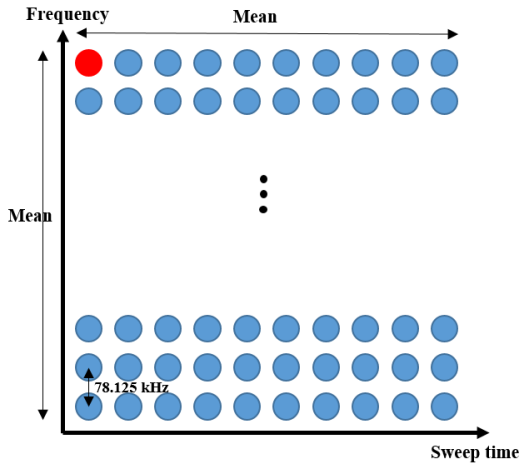

Fig. 9. Data processing for one small grid.

inversed about the propagation distance:

$$PL(f_c, d)[\text{dB}] = A + 10n\log_{10}(d) + B(f_c) + X. \quad (36)$$

Here, PL indicates the power loss in the dB scale after range d propagation. In addition, A and B are offsets due to the near-field radiation and center frequency f_c. Moreover, X is the shadow fading modeled as a random distribution, and n is the path loss exponent that determines the accuracy of the model in performing ranging. Generally, the values of A, B, and n and the statistical characteristics of X are defined with actual site measurements. Our proposed model was compared to the Indoor Hotspot models of WINNER II [8], 3GPP [9], and the free space model that does not consider propagation environments.

Figs. 10, 11, and 12 represent the measurement and modeling results of hallways 1, 2, and 3. The red points indicate the measured values in small grids. The averaged data in small grids are utilized for the ranging process at each large grid. Because existing PMs do not consider the roughness of materials, their slopes (i.e., the degree of power loss) are hardly influenced by the frequency and measurement site. For example, existing models have the same slope in hallways 1 and 3 even though hallway 3 has a much smoother wall that is closer to the ideal waveguide. Unlike these existing models, the proposed PM sufficiently captures the smoothness

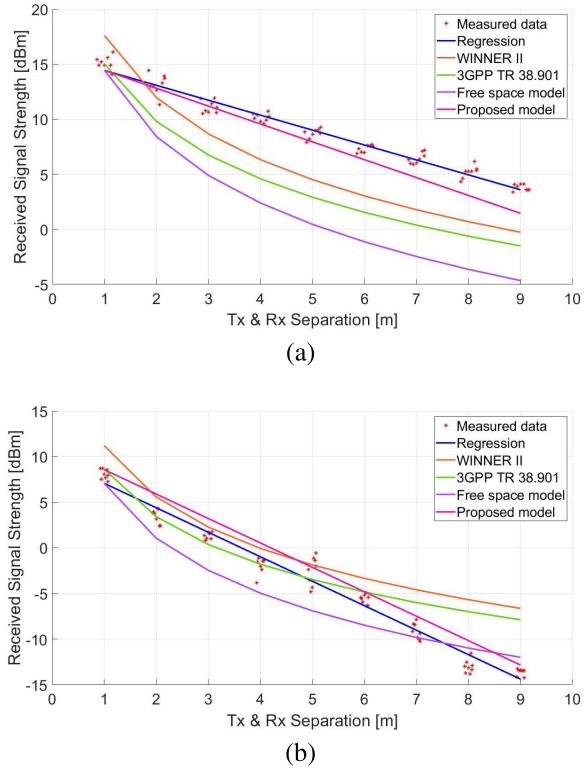

Fig. 10. Measurement and modeling results in Hallway 1. (a) 2.4–2.48-GHz band. (b) 5.17–5.33-GHz band.

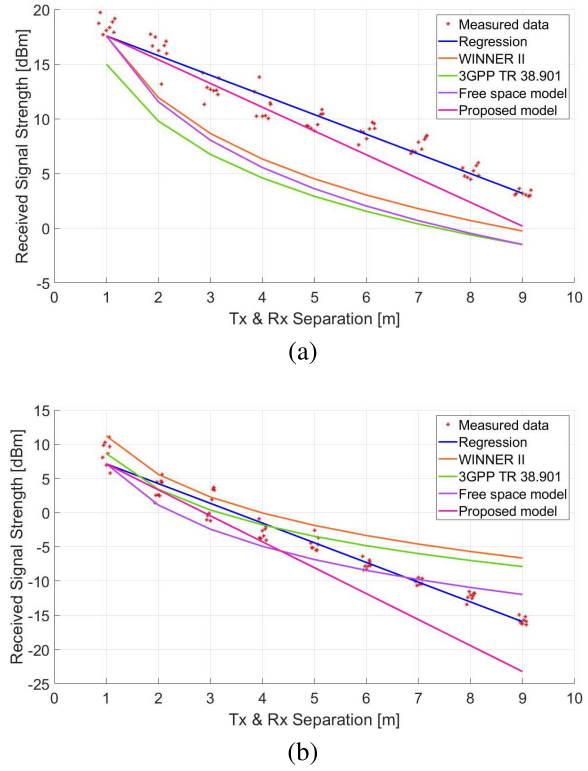

Fig. 11. Measurement and modeling results in Hallway 2. (a) 2.4–2.48-GHz band. (b) 5.17–5.33-GHz band.

of the sidewall in hallway 3. Moreover, in hallway 2, which has the roughest wall in the INMC building, the measured signal strength decreases rapidly at the 5-GHz band. The proposed

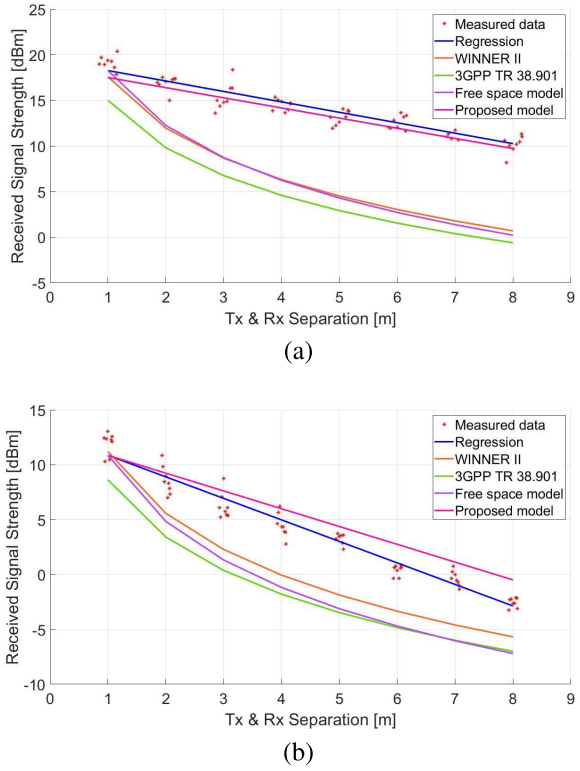

Fig. 12. Measurement and modeling results in Hallway 3. (a) 2.4–2.48-GHz band. (b) 5.17–5.33-GHz band.

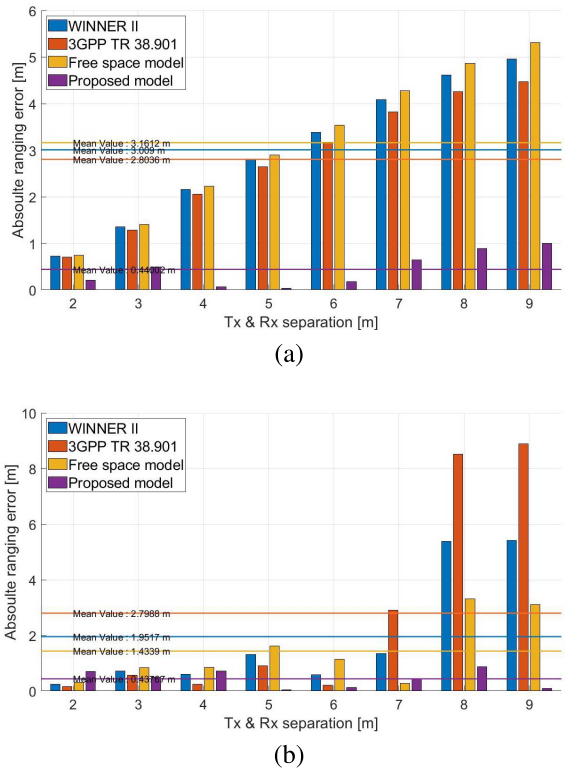

Fig. 13. Ranging errors with considered models in Hallway 1. (a) 2.4–2.48-GHz band. (b) 5.17–5.33-GHz band.

model solely follows this tendency, which indicates that the proposed model is more appropriate in rough-wall environments. The measurement results imply that the attenuation difference according to the frequency bands increases with the roughness of the wall. While conventional models cannot capture this difference sufficiently, the proposed model recognizes the difference. The ranging process with the measured data and its results are presented in the remainder of this section.

D. Ranging Results

In every hallway, the measured signal strength of the first large grid (i.e., 1-m transceiver separation) is used for the reference signal strength P_0. Because far-field radiation is assumed with the reference distance manner, existing models conduct ranging processes only with the parameter n. At each large grid, ranging errors of considered models are compared with each other.

Fig. 13 represents the ranging results in hallway 1. At both bands, the proposed model exhibits submeter-ranging errors. Even though existing models have reasonable performances, which is 2–3-m average ranging error, they are vulnerable to rough-wall environments. This weakness becomes prominent in high-frequency and far-propagation situations by causing an over-5-m ranging error, which is found by the result at the 5-GHz band. Conversely, the proposed model provides centimeter-scale ranging errors in the same situations. The ranging results in hallway 2 are also shown in Fig. 14. Similar to hallway 1, the proposed model presents a sufficient performance. It shows a 0.5423-m average ranging error at the

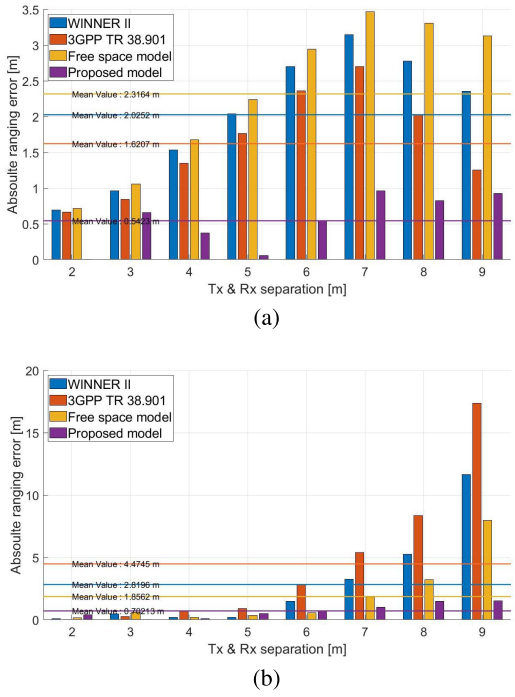

Fig. 14. Ranging errors with considered models in Hallway 2. (a) 2.4–2.48-GHz band. (b) 5.17–5.33-GHz band.

2.4-GHz band and 0.7021 m at the 5-GHz band. Because hallway 2 has the roughest wall in the INMC building, the ranging performances with existing models are highly degraded at the

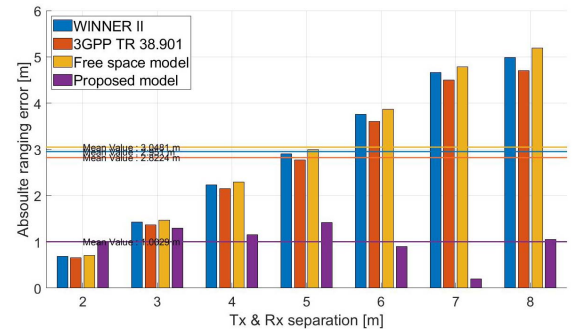

(a)

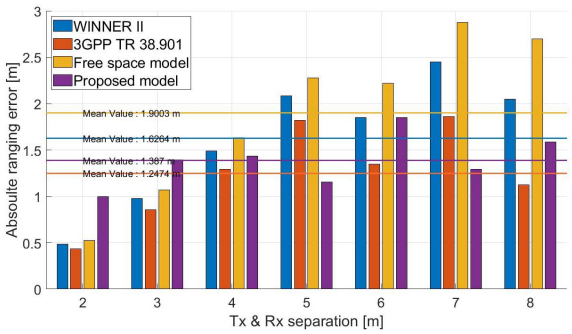

(b)

Fig. 15. Ranging errors with considered models in Hallway 3. (a) 2.4–2.48-GHz band. (b) 5.17–5.33-GHz band.

TABLE II
MEAN RANGING ERRORS WITH PMS IN EACH HALLWAY

	WINNER II	3GPP	Free space	Proposed
Hallway 1 (2.4 GHz)	3.009 m	2.804 m	3.161 m	0.440 m
Hallway 1 (5 GHz)	1.952 m	2.799 m	1.434 m	0.438 m
Hallway 2 (2.4 GHz)	2.025 m	1.621 m	2.316 m	0.542 m
Hallway 2 (5 GHz)	2.820 m	4.475 m	1.856 m	0.702 m
Hallway 3 (2.4 GHz)	2.951 m	2.822 m	3.048 m	1.003 m
Hallway 3 (5 GHz)	1.626 m	1.247 m	1.900 m	1.387 m
Mean value	2.397 m	2.628 m	2.286 m	0.752 m

5-GHz band compared to the 2.4-GHz band. However, the proposed model achieves the submeter-ranging performances regardless of the frequency band. Finally, Fig. 15 provides the ranging results in hallway 3. Here, the proposed model gives a 1.003-m average ranging error at the 2.4-GHz band and 1.387 m at the 5-GHz band. Compared to other hallways, performance degradation occurs in Hallway 3 even though the ranging performance is better than the existing models. These results indicate that the proposed model is more effective in waveguide-shaped structures that have an adequate L value.

Mean ranging errors in each hallway and their total average values are given in Table II. Three existing models have 2.397-, 2.626-, and 2.286-m ranging errors, respectively, whereas the proposed model has a 0.752-m ranging error. At the 5-GHz band, the free space model often shows better performance than the other empirical models because the free space model having the highest path loss exponent follows a rapid power decrease in rough-wall environments. However, at the 2.4-GHz band, which can be considered as relatively smooth-wall environments, empirical models show satisfactory performance. The proposed model considering the roughness of the propagation environment has submeter-ranging performance regardless of the frequency band.

V. CONCLUSION

In this article, we proposed an effective PM for RSS-based ranging in indoor hallways. The indoor hallway environment was modeled with a slab waveguide based on the waveguide theory. The proposed model took into account the roughness of practical indoor structures, which has not been considered in the existing channel models. Moreover, in comparison with an ideal waveguide that completely retains guided power, power leakage occurs in practical indoor hallways. Thus, the proposed model considers this phenomenon by designing parameters for the penetration loss. Because the proposed model has a form that can be easily inversed about the propagation distance, signal strength-based ranging can be conducted efficiently. Finally, the effectiveness of the proposed model was validated through actual site experiments at the two frequency bands that are most discussed for indoor applications in wireless communication areas. To collect various signal strength data according to the propagation distance, the channel-sounding system based on the VNA was configured. The proposed model exhibited submeter-ranging performances, which is better than those of conventional channel models commonly used for RSS-based ranging.

REFERENCES

[1] Y. Kim, B. Lee, H. So, and S.-C. Kim, "Localization technique considering position uncertainty of reference nodes in wireless sensor networks," *IEEE Sensors J.*, vol. 18, no. 3, pp. 1324–1332, Feb. 2018.
[2] A. Makki, A. Siddig, and C. J. Bleakley, "Robust high resolution time of arrival estimation for indoor WLAN ranging," *IEEE Trans. Instrum. Meas.*, vol. 66, no. 10, pp. 2703–2710, Oct. 2017.
[3] T. Wang, H. Xiong, H. Ding, and L. Zheng, "A hybrid localization algorithm based on TOF and TDOA for asynchronous wireless sensor networks," *IEEE Access*, vol. 7, pp. 158981–158988, 2019.
[4] E. Tuba, M. Tuba, and M. Beko, "Node localization in ad hoc wireless sensor networks using fireworks algorithm," in *Proc. 5th Int. Conf. Multimedia Comput. Syst. (ICMCS)*, Sep. 2016, pp. 223–229.
[5] S. B. Cruz, T. E. Abrudan, Z. Xiao, N. Trigoni, and J. Barros, "Neighbor-aided localization in vehicular networks," *IEEE Trans. Intell. Transp. Syst.*, vol. 18, no. 10, pp. 2693–2702, Oct. 2017.
[6] H. A. Khattak, S. U. Islam, I. U. Din, and M. Guizani, "Integrating fog computing with VANETs: A consumer perspective," *IEEE Commun. Standards Mag.*, vol. 3, no. 1, pp. 19–25, Mar. 2019.
[7] M. N. Semeria, "Symbiotic low-power, smart and secure technologies in the age of hyperconnectivity," in *IEDM Tech. Dig.*, Dec. 2016, pp. 1.3.1–1.3.14.
[8] IST-WINNER, I. I. Deliverable 1.1. 2 v. 1.2, "WINNER II channel models," IST-WINNER2, Tech. Rep., 2007.

[9] *Study on Channel Model for Frequencies From 0.5 to 100 GHz*, document TR 38.901, 3GPP, 2017.
[10] *Study on Channel Model for Frequency Spectrum Above 6 GHz*, document TR 38.900, 3GPP, 2016.
[11] M. K. Samimi and T. S. Rappaport, "3-D millimeter-wave statistical channel model for 5G wireless system design," *IEEE Trans. Microw. Theory Techn.*, vol. 64, no. 7, pp. 2207–2225, Jul. 2016.
[12] J.-Y. Lee, Y. Kim, S. Lee, W. Cho, and S.-C. Kim, "Estimation of room shape using radio propagation channel analysis," *IEEE Sensors J.*, vol. 19, no. 24, pp. 12316–12324, Dec. 2019.
[13] P.-H. Tseng, Y.-C. Chan, Y.-J. Lin, D.-B. Lin, N. Wu, and T.-M. Wang, "Ray-tracing-assisted fingerprinting based on channel impulse response measurement for indoor positioning," *IEEE Trans. Instrum. Meas.*, vol. 66, no. 5, pp. 1032–1045, May 2017.
[14] D. Porrat and D. C. Cox, "UHF propagation in indoor hallways," *IEEE Trans. Wireless Commun.*, vol. 3, no. 4, pp. 1188–1198, Jul. 2004.
[15] J. Leung, "Hybrid waveguide theory-based modeling of indoor wireless propagation," Ph.D. dissertation, Dept. Elect. Comput. Eng., Univ. Toronto, Toronto, ON, Canada, 2009.
[16] D. M. Pozar, *Microwave Engineering*. Hoboken, NJ, USA: Wiley, 2011.
[17] S. O. Kasap, *Optoelectronics and Photonics: Principles and Practices*. Upper Saddle River, NJ, USA: Prentice-Hall, 2001.
[18] J. P. R. Lacey and F. P. Payne, "Radiation loss from planar waveguides with random wall imperfections," *IEE Proc. J Optoelectron.*, vol. 137, no. 4, pp. 282–288, Aug. 1990.
[19] G. Ames and D. Hall, "Attenuation in planar optical waveguides: Comparison of theory and experiment," *IEEE J. Quantum Electron.*, vol. JQE-19, no. 5, pp. 845–853, May 1983.
[20] *IEEE Standard for Information Technology–Telecommunications and Information Exchange Between Systems–Local and Metropolitan Area Networks–Specific Requirements—Part 11: Wireless LAN Medium Access Control (MAC) and Physical Layer (PHY) Specifications Amendment 6: Wireless Access in Vehicular Environments*, Standard 802.11, 2010.
[21] L. Banin, O. Bar-Shalom, N. Dvorecki, and Y. Amizur, "Scalable Wi-Fi client self-positioning using cooperative FTM-sensors," *IEEE Trans. Instrum. Meas.*, vol. 68, no. 10, pp. 3686–3698, Oct. 2019.
[22] J. Yoo, K. H. Johansson, and H. Jin Kim, "Indoor localization without a prior map by trajectory learning from crowdsourced measurements," *IEEE Trans. Instrum. Meas.*, vol. 66, no. 11, pp. 2825–2835, Nov. 2017.
[23] A. Alhosainy, K. M. Attiah, R. H. Gohary, and I. Lambadaris, "Statistical evaluation of the behavior of 5-GHz radio LAN devices," *IEEE Trans. Instrum. Meas.*, vol. 69, no. 4, pp. 1103–1117, Apr. 2020.
[24] N. Pinel, C. Bourlier, and J. Saillard, "Degree of roughness of rough layers: Extensions of the Rayleigh roughness criterion and some applications," *Prog. Electromagn. Res. B*, vol. 19, pp. 41–63, 2010.
[25] V. F. Mikhailov, "Radiation of a flat waveguide closed by molted heat protection," in *Proc. Wave Electron. Appl. Inf. Telecommun. Syst. (WECONF)*, Jun. 2019, pp. 1–4.
[26] M. K. Olkkonen, V. Mikhnev, and E. Huuskonen-Snicker, "Complex permittivity of concrete in the frequency range 0.8 to 12 GHz," in *Proc. 7th Eur. Conf. Antennas Propag. (EuCAP)*, Apr. 2013, pp. 3319–3321.

Kyoung-Min Park received the B.S. degree in electrical and computer engineering from Ajou University, Suwon, South Korea, in 2016. He is currently pursuing the Ph.D. degree in electrical engineering and computer science with Seoul National University, Seoul, South Korea.

His research interests include sensor network localization, propagation channel modeling, wireless channel measurements, and analysis of wave propagation.

Seong-Hwan Hyun received the B.S. degree from the Division of Electronics and Electrical Engineering, Dongguk University, Seoul, South Korea, in 2018. He is currently pursuing the Ph.D. degree in electrical engineering and computer science with Seoul National University, Seoul.

His current research interests include wireless channel modeling, sensor network localization, V2X communications, and systems of engineering of wireless systems.

Seongwook Lee (Member, IEEE) received the B.S. and Ph.D. degrees in electrical and computer engineering from Seoul National University (SNU), Seoul, Republic of Korea, in February 2013 and August 2018, respectively.

From September 2018 to February 2020, he has worked as a Staff Researcher with the Machine Learning Laboratory, AI & SW Research Center, Samsung Advanced Institute of Technology (SAIT), Suwon, Republic of Korea. Since March 2020, he has been an Assistant Professor with the School of Electronics and Information Engineering, College of Engineering, Korea Aerospace University, Goyang, Republic of Korea. His research interests include radar signal processing techniques, machine learning applications for radio technology, and wireless communications.

Dr. Lee received the Distinguished Ph.D. Dissertation Award from the Department of Electrical and Computer Engineering, SNU.

Seong-Cheol Kim (Senior Member, IEEE) received the B.S. and M.S. degrees from Seoul National University, Seoul, South Korea, in 1984 and 1987, respectively, and the Ph.D. degree from the Polytechnic Institute, New York University (NYU), Brooklyn, NY, USA, in 1995, all in electrical engineering.

From 1995 to 1999, he was with the Wireless Communications Systems Engineering Department, AT&T Bell Laboratories, Holmdel, NJ, USA. Since 1999, he has been a Professor with the Department of Electrical and Computer Engineering, Seoul National University. His current research interests include wireless communication systems, including millimeter-wave channel modeling, wireless localization algorithms, acoustic channel modeling, wireless channel measurements, and automotive radar signal processing.